Supplementary data

Supplementary Table S1. *HACE1* mutational landscape in human cancer.

HACE1 mutations, including missense, nonsense, frameshift mutations, splice site mutations that occur in an intron (in a splice acceptor or donor site), splice region mutations that occur near the intron/exon junction, and protein-protein fusions, in individual cancer types as available from the cBioPortal and TGen datasets.

Supplementary Figure S1

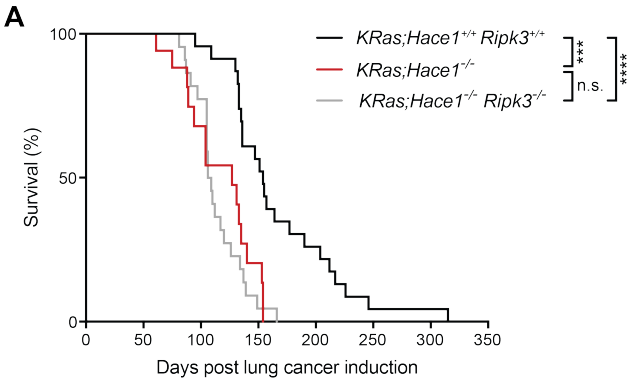

Supplementary Figure S1. Loss of *Hace1* results in increased lung tumorigenesis independent of RIPK3.

(A) Kaplan-Meier survival curves of $KRas^{G12D};Hace1^{+/+}Ripk3^{+/+}$ (n=23), $KRas^{G12D};Hace1^{-/-}$ (n=15) and $KRas^{G12D};Hace1^{-/-}Ripk3^{-/-}$ (n=22) mice. Upon intratracheal instillation of Adeno-Cre on day 0, mice carrying the conditional *Lox-Stop-Lox* (*LSL*)-$KRas^{G12D}$ allele develop lung adenocarcinomas due to the removal of the Stop cassette and the induction of oncogenic $KRas^{G12D}$. *** P<0.001, **** P<0.0001, ns (not significant) (log-rank test).

Supplementary Figure S2

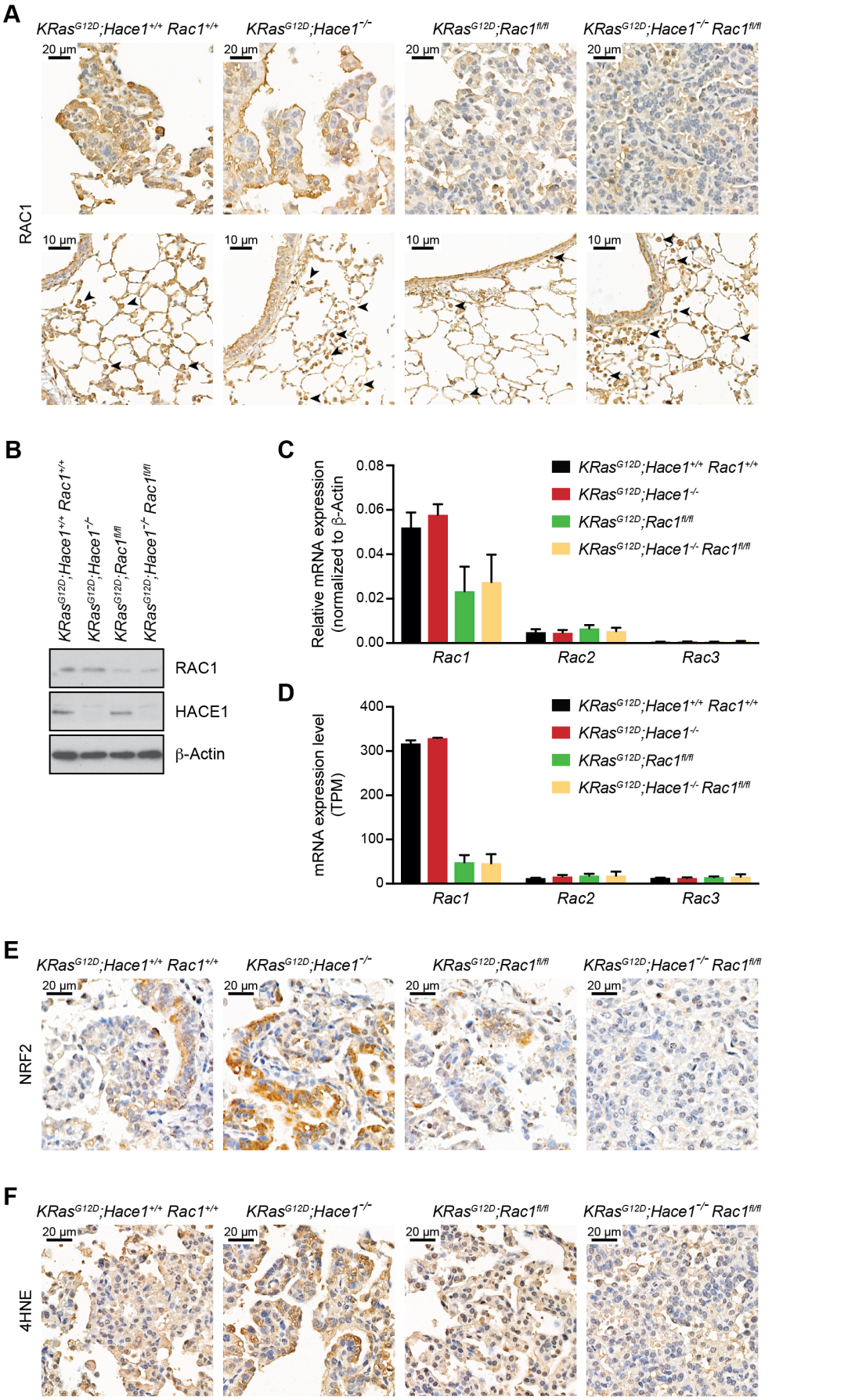

Supplementary Figure S2. Analysis of RAC, NRF2 and 4HNE expression.

(A) Representative pictures of RAC1 immunostaining of lungs at week 14 post lung cancer induction for *KRas^{G12D};Hace1$^{+/+}$Rac1$^{+/+}$*, *KRas^{G12D};Hace1$^{-/-}$*, *KRas^{G12D};Rac1$^{fl/fl}$* and *KRas^{G12D};Hace1$^{-/-}$Rac1$^{fl/fl}$* mice. The upper panels show RAC1 expression in tumor tissue, the lower panels show RAC1 expression in adjacent tissue. Macrophages are indicated (black arrows). Scale bars, 20µm or 10µm. **(B-C)** Lung tumor cells were isolated from *KRas^{G12D};Hace1$^{+/+}$Rac1$^{+/+}$*, *KRas^{G12D};Hace1$^{-/-}$*, *KRas^{G12D};Rac1$^{fl/fl}$* and *KRas^{G12D};Hace1$^{-/-}$Rac1$^{fl/fl}$* mice at week 12 post lung cancer induction. (B) Immunoblotting for RAC1, HACE1, and β-Actin as loading control. Representative Western blots are shown. (C) qRT-PCR analysis of *Rac1*, *Rac2* and *Rac3* mRNA expression (n≥4). **(D)** Relative *Rac1*, *Rac2* and *Rac3* mRNA expression (TPM) in primary pneumocytes isolated from *KRas^{G12D};Hace1$^{+/+}$Rac1$^{+/+}$*, *KRas^{G12D};Hace1$^{-/-}$*, *KRas^{G12D};Rac1$^{fl/fl}$* and *KRas^{G12D};Hace1$^{-/-}$Rac1$^{fl/fl}$* mice. Purified pneumocytes were infected with Adeno-Cre for 4 days to delete *Rac1*. Relative expression levels were determined in triplicate (except for *KRas^{G12D};Hace1$^{-/-}$Rac1$^{fl/fl}$* mice: n=2) and are shown compared to *KRas^{G12D};Hace1$^{+/+}$Rac1$^{+/+}$* control cells (values set to 1). Representative pictures of **(E)** NRF2 and **(F)** 4HNE immunostaining of lungs at week 16 post lung cancer induction for *KRas^{G12D};Hace1$^{+/+}$Rac1$^{+/+}$*, *KRas^{G12D};Hace1$^{-/-}$*, *KRas^{G12D};Rac1$^{fl/fl}$* and *KRas^{G12D};Hace1$^{-/-}$Rac1$^{fl/fl}$* mice. Scale bars, 20µm. Data in (B) are presented as mean values ± SEM.

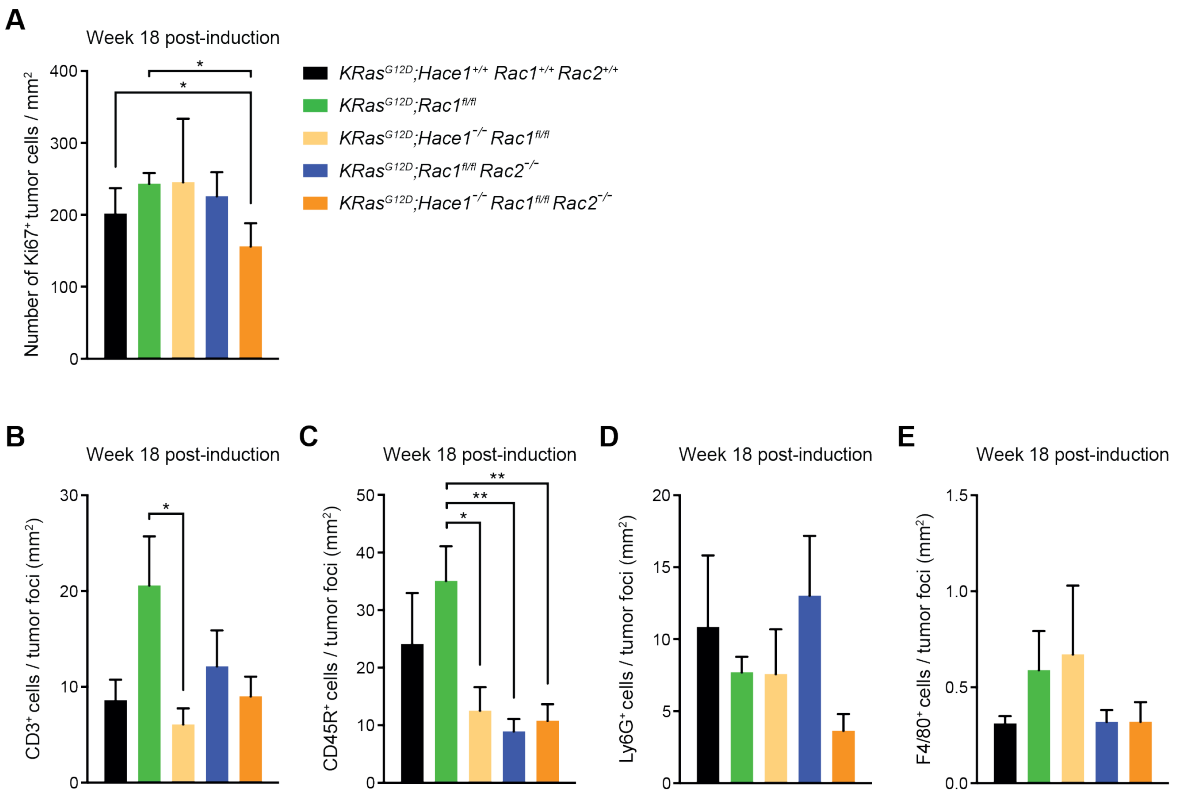

Supplementary Figure S3. Analysis of tumor microenvironment.

Immunohistochemical analysis at week 18 post lung cancer induction for *KRas^{G12D};Hace1$^{+/+}$Rac1$^{+/+}$Rac2$^{+/+}$*, *KRas^{G12D};Rac1$^{fl/fl}$*, *KRas^{G12D};Hace1$^{-/-}$Rac1$^{fl/fl}$*, *KRas^{G12D};Rac1$^{fl/fl}$Rac2$^{-/-}$* and *KRas^{G12D};Hace1$^{-/-}$Rac1$^{fl/fl}$Rac2$^{-/-}$* mice. Slides are derived from the same experiment shown in Fig. 5E,F. **(A)** Quantification of Ki67^{+} tumor cells. **(B-E)** Quantification of CD3^{+} T cells (B), CD45R^{+} B cells (C), Ly6G^{+} neutrophils (D) and F4/80^{+} macrophages (E) within the tumors of *KRas^{G12D};Hace1$^{+/+}$Rac1$^{+/+}$Rac2$^{+/+}$*, *KRas^{G12D};Rac1$^{fl/fl}$*, *KRas^{G12D};Hace1$^{-/-}$Rac1$^{fl/fl}$*, *KRas^{G12D};Rac1$^{fl/fl}$Rac2$^{-/-}$* and *KRas^{G12D};Hace1$^{-/-}$Rac1$^{fl/fl}$Rac2$^{-/-}$* mice. * P<0.05, ** P<0.01 (One-way ANOVA, Tukey's post-hoc test, n≥5 mice per cohort). Data are presented as mean values ± SEM.

Supplementary Figure S4

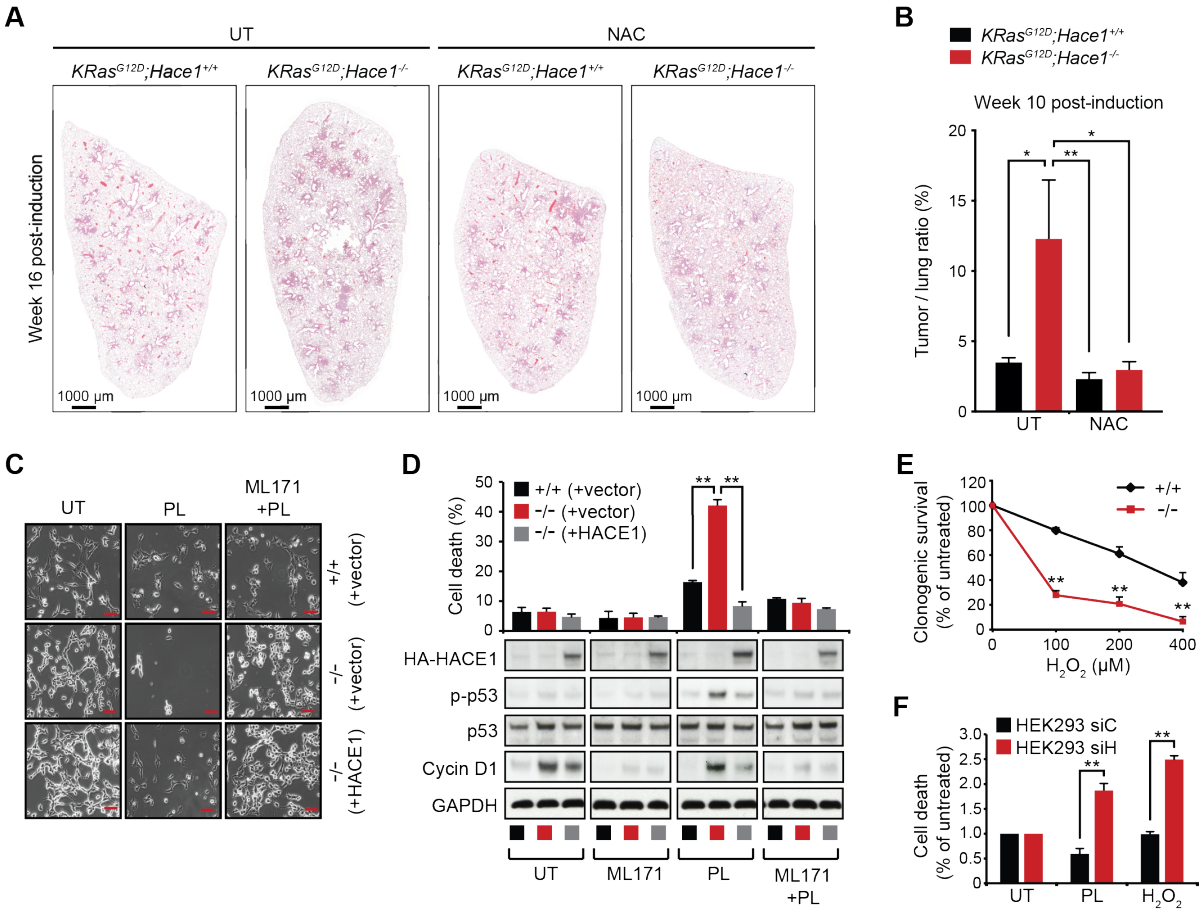

Supplementary Figure S4. Treatment of *KRas^{G12D};Hace1$^{-/-}$* mice with a ROS scavenger diminishes lung tumorigenesis and *Hace1*-deficient cells are sensitive to exogenous induction of oxidative stress.

(A-B) *KRas^{G12D};Hace1$^{+/+}$* and *KRas^{G12D};Hace1$^{-/-}$* were treated with NAC or left untreated (UT) starting 9 days post lung cancer induction with Adeno-Cre (4x10^{10} pfu/ml). **(A)** Representative pictures of haematoxylin and eosin (H&E) stained-lung sections and **(B)** tumor-to-lung ratios at week 10 post lung cancer induction for untreated and NAC-treated *KRas^{G12D};Hace1$^{+/+}$* and *KRas^{G12D};Hace1$^{-/-}$* mice. Scale bars, 1 mm for 10x images and 50µm for 40x images of lung sections. * P<0.05, ** P<0.01 (One-way ANOVA, Tukey's post-hoc test, n≥5 mice per cohort). **(C)** Phase contrast images of *Hace1* wildtype (+/+) and KO (-/-) MEFs reconstituted with empty vector or wildtype *Hace1*, 72 h post treatment with the ROS-inducer piperlongumine (PL - 1 µM) and the NOX1 inhibitor ML171 [10 µM] as indicated. Scale bars, 10µm. **(D)** Percent cell death (top) and expression of indicated proteins (bottom, determined by Western blotting) of *Hace1* wildtype (+/+) and KO (-/-) MEFs reconstituted with empty vector or wildtype *Hace1*, left untreated (UT) or 49 h post-treatment with PL [1

μM] and/or ML171 [10 μM] as indicated. ** P<0.001 (Student's two-tailed *t*-test, n=3). **(E)** Clonogenic survival of *Hace1* wildtype (+/+) and KO (-/-) MEFs treated with indicated concentrations of H_2O_2 relative to untreated cells. Clonogenic survival was determined on day 7 after H_2O_2 treatment in triplicate cultures. ** P<0.001 (Student's two-tailed *t*-test, n=3). **(F)** Cell death of HEK293 cells 72 h after transfection with control (siC) or *HACE1* (siH) siRNAs, left untreated (UT) or 48 h post-treatment PL [1 μM] or H_2O_2 [50 μM]. Cell death was determined on day 2 after PL or H_2O_2 treatment in triplicate cultures. ** P<0.001 (Student's two-tailed *t*-test, n=3). Data in (B), (C) and (D) are presented as mean values ± SEM.

Supplementary methods

Immunohistochemistry. The following primary antibodies were also used: rabbit polyclonal anti-CD3 (Abcam, ab49943, 1:3000 dilution), rat monoclonal anti-CD45R (BD Pharmingen, 550286, 1:50 dilution), rat monoclonal anti-Ly6G (BioLegend, 127601, 1:500 dilution), rat monoclonal anti-F4/80 (Bio-Rad, MCA497G, 1:100 dilution), rabbit polyclonal anti-RAC1 (Invitrogen, PA1-091, 1:50 dilution), rabbit polyclonal anti-4HNE (Abcam, ab46545, 1:200) and rabbit polyclonal anti-NRF2 (Abcam, ab31163, 1:100). CD3, CD45R, Ly6G, F4/80 were automatically evaluated by an algorithm programmed and executed using the Definiens Developer software suite. Representative IHC images were selected from scans of the 3D Histech Pannoramic Flash II.

Isolation and culture of primary pneumocytes. Primary pneumocytes were purified as described (1,2). In brief, lungs were dissected from 8–12-week-old mice, infused with IMDM containing 600 U/mL collagenase IV (Worthington) and 200 U/mL DNase (Worthington) through the trachea, and incubated for 1 h at 37°C. After the isolation, cells were maintained in Ham's F-12 media supplemented with 15 mM HEPES, 0.8 mM $CaCl_2$, 0.25% BSA, ITS (Sigma) and 2% FCS, at 37ºC and 5% CO_2 conditions. Cells were infected with Adeno-Cre (MOI = 100) *in vitro* for 2 h at 37°C and harvested after 4 days of culture.

RAC1 activation assay. Primary lung tumor cells were serum starved for 6 h and then stimulated with 50 ng/ml EGF for 5 min. Clarified cell lysates with equal protein concentrations were affinity precipitated for 1 h at 4°C using GST-PBD-containing glutathione agarose resin. The resin was washed and boiled in Laemmli buffer to remove bound proteins. Active GTP-RAC1 was detected by immunoblotting with mouse anti-RAC1 antibody (Cytoskeleton). For positive and negative controls for active and inactive RAC1, the non-hydrolysable GTP analog GTPγS and GDP were used, respectively. Cell lysates were loaded with 100 µM GTPγS or 1 mM GDP in the presence of 10 mM EDTA for 15 min at 30°C. To terminate the reaction, the lysates were placed on ice and supplemented with 60 mM $MgCl_2$. These control samples were then incubated with the GST-PBD-containing resin and further processed in the same manner as the other samples.

***In vitro* clonogenic survival and cell death assays**. For clonogenic survival assays (3), MEFs were seeded in 6 cm dishes (5,000 cells/dish) and treated with H_2O_2 as indicated. After visualization with crystal violet, live cells were counted on the NC-3000 nucleocounter (ChemoMetec). To assess cell death after treatment with PL and ML171, cells were stained with 2.5 μg/mL Hoechst 33342 (Molecular Probes, Invitrogen) and cells containing condensed nuclei were counted using an inverted Olympus (Center Valley, PA) IX-70 fluorescent microscope (Filter U-MWU, 330–385 nm) connected to an Olympus C-3030 digital camera. For each experiment, a minimum of six areas with at least 30 cells each were randomly chosen and counted. The same microscope settings were used to take representative phase-contrast images of the cells.

Quantitative RT–PCR. Total RNA from the primary pneumocytes and lung tumor cells was extracted using Trizol (Invitrogen). cDNA was synthesized using iScript™ cDNA Synthesis Kit (BioRad). qRT-PCR was performed with iQ™ SYBR® Green Supermix (BioRad) and gene-specific primers using CFX Real-Time PCR Detection Systems (BioRad). The following primers were used: *Rac1* fwd: ACA CCA CTG TCC CAA TA CTC C, rev: GCA CTC CAG GTA TTT GAC AGC; *Rac2* fwd: GGA CAC CAT CGA GAA GCT GA, rev: GGT CTT CAG GCC TCG CTG; *Rac3* fwd: GAC AAG AAG CTG GCA CCC A, rev: GCC TCG TCG AAC ACT GTC TT. The data were analyzed by relative ΔΔCT quantification method using *Gapdh* CT values as internal reference in each sample.

References

1. Schramek D, Kotsinas A, Meixner A, Wada T, Elling U, Pospisilik JA, et al. The stress kinase MKK7 couples oncogenic stress to p53 stability and tumor suppression. Nat Genet. Nature Publishing Group; 2011;43:212–9.

2. Rao S, Sigl V, Wimmer RA, Novatchkova M, Jais A, Wagner G, et al. RANK rewires energy homeostasis in lung cancer cells and drives primary lung cancer. Genes & Development. Cold Spring Harbor Lab; 2017;31:2099–112.

3. Daugaard M, Baude A, Fugger K, Povlsen LK, Beck H, Sørensen CS, et al. LEDGF (p75) promotes DNA-end resection and homologous recombination. Nat Struct Mol Biol. Nature Publishing Group; 2012;19:803–10.